Spin trajectory along an evanescent loop in zinc-blende semiconductors

T. L. Hoai Nguyen,[1,2] Henri-Jean Drouhin,[1,*] and Guy Fishman[2]
[1]*Ecole Polytechnique, LSI, CNRS and CEA/DSM/IRAMIS, Palaiseau F-91128, France*
[2]*Université Paris-Sud, IEF, CNRS, Orsay F-91405, France*
(Received 20 May 2009; revised manuscript received 8 July 2009; published 21 August 2009)

Due to the absence of inversion symmetry, spin-orbit interaction leads to a very particular topology of the evanescent states in zinc-blende semiconductors, which may consist of loops connecting different spin sub-bands at the zone center. The spin-vector motion along such loops is analytically or numerically studied. A surprising picture emerges from this detailed analysis. Namely, the two spin sub-bands do *not* correspond to opposite spin states near the Brillouin-zone center and merge with identical spins at larger wave vector. This determines the spin-filtering capabilities of the semiconductor barrier.

DOI: 10.1103/PhysRevB.80.075207 PACS number(s): 72.25.Dc, 73.40.Gk, 71.20.Mq

I. INTRODUCTION

Spin-dependent tunneling is of growing importance in spintronics.[1] Fundamental properties of tunneling phenomena in solids are intensively investigated and the structure of the evanescent states is crucial in determining the tunneling scheme. In pioneering papers, Heine[2] and Jones[3] have derived general properties of the complex bands. The evanescent states, which are associated with complex wave vectors, have to be visualized in a real six-dimensional vectorial space, instead of the familiar three-dimensional representation of the real band structure. A careful study of the evanescent band structure inside the band gap of zinc-blende semiconductors can be found in Refs. 4 and 5. This semiconductor family, which is of great technological importance, is a paradigm for fundamental spin physics because a very accurate analytical description of the relevant bands can be obtained. Due to the absence of inversion symmetry, it is well-known that the spin-orbit interaction removes the spin degeneracy of the bands.[6] Concerning the evanescent states, a particular structure arises with a deeply directional dependent nature. Its implications for tunneling have been extensively investigated in Ref. 7, paving the way to spin-orbit engineering of heterostructures. There, it was also shown that even the familiar notion of probability current has to be revisited in the presence of a D'yakonov-Perel' (DP) field,[8] as well as the matching conditions of the wave function at the boundaries. Perel' *et al.*[9] pointed out that a [001]-oriented tunnel barrier under off-normal incidence presents spin-filtering capabilities. These properties are related to the particular topology of the evanescent states in the fundamental band gap which, along the relevant directions, consist of loops connecting two different spin sub-bands at the zone center.[4,5] In the present paper we study the spin properties and especially the spin-vector trajectory along such loops. This provides us with a tractable case where a number of general considerations[2,3] find illuminating illustrations and it emphasizes that, when dealing with spin-dependent tunneling properties, one has to be extremely cautious because the regular representations do not apply.

In zinc-blende semiconductors, the spin splitting of the first conduction band is usually studied near the Brillouin-zone center and described through an effective (2×2) Hamiltonian, referred to as the DP Hamiltonian.[8] In Ref. 4, the evanescent band structure of GaAs was calculated within the $\mathbf{k}\cdot\mathbf{p}$ framework, incorporating an increasing number of bands. Starting with the DP Hamiltonian the evanescent band structure was finally calculated through a (30×30) Hamiltonian formalism which had been shown to yield an accurate description of the first and second real conduction bands and of the three upper real valence bands over the whole Brillouin zone. Concerning the evanescent states in the fundamental band gap (between the top of the upper valence bands and the bottom of the first conduction band) we are interested in, because their wave-vector extension is limited—less than about 10 % of the Brillouin zone—it is sufficient to use a (14×14) Hamiltonian[4] which is also the smallest possible which can include the matrix elements responsible for the spin splitting. This description takes into account seven orbital states, the three *p*-like bonding states which give rise to the three upper valence bands (Γ_{5V}), the *s*-like antibonding states which give rise to the first conduction band (Γ_1), and the three *p*-like antibonding states which correspond to the second conduction band (Γ_{5C}). For directions of the type $[\xi,0,iK]$ $(\xi,K\geq 0)$, referred to the cubic crystallographic axes, the evanescent states consist of loops as shown in Fig. 1, provided that $0\leq\theta<45°$ where $\tan\theta=\xi/K$.[4] The loop extension in wave-vector space decreases when θ increases, tending to zero when θ approaches 45°.

The purpose of the present paper is to study the direction of the two spin states along a whole loop. This is simple and analytical near the Brillouin-zone center (in a small energy domain just below the bottom of the first conduction band), where the (2×2) DP Hamiltonian is sufficient, while the (14×14) Hamiltonian, needed to describe the whole loop, needs numerical resolution.

II. SPIN-VECTOR CALCULATION

The general expression of a normalized pure spin state is $|\phi\rangle=a\uparrow+b\downarrow$, $|a|^2+|b|^2=1$, a combination with complex scalar coefficients of $\uparrow$, $\downarrow$, which are the eigenvectors of $\hat{\sigma}_z$, the z component of the Pauli operator $\hat{\boldsymbol{\sigma}}$. The spin vector is given by the mean value of the Pauli operator $\hat{\boldsymbol{\sigma}}$ in the state $|\phi\rangle$, i.e., $\langle\phi|\hat{\sigma}_j|\phi\rangle$, $j=x,y,z$, with $\langle\phi|\hat{\boldsymbol{\sigma}}|\phi\rangle^2=\Sigma_j\langle\phi|\hat{\sigma}_j|\phi\rangle^2=1$.

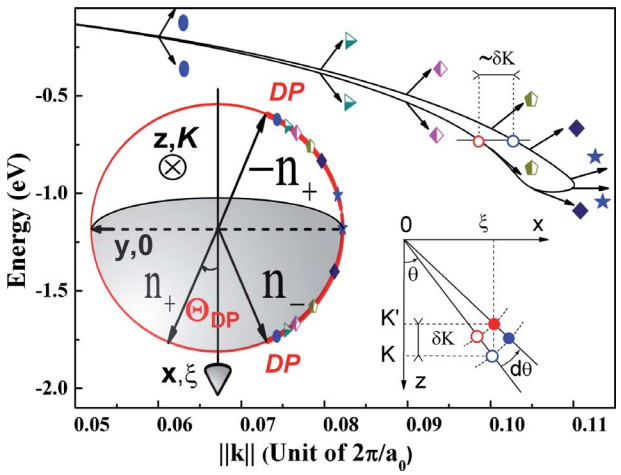

FIG. 1. (Color online) Evanescent loop in the wave vector—energy plane. The energy origin is set at the bottom of the first conduction band. The wave-vector $\mathbf{k}$ lies along the $[\tan\theta,0,i]$ direction, at $\eta=\xi/K=0.4$ ($\theta=21.8°$). The spin vector, in the xOy plane, is represented, after a numerical calculation, for several pairs of points (identical symbols) related to the two sub-bands at a given wave vector. For small wave vectors—in the D'yakonov-Perel limit (out of the representation domain)—the spin vector is given by n_- (respectively, $-n_+$) for the lower-(respectively, upper-) energy band. Lower right inset: top view of the intercepts of two evanescent loops with a constant energy plane determining the evanescent components of the wave-vector K and K' at constant ξ. To the first order, the wave-vector change δK can be directly measured on the loop in the main figure. Lower left inset: the unit sphere allows a simple visualization of the spin-direction trajectory along the loop (take care that the sphere is pointing down to the north hemisphere, the axis being along Ox, the spin-filter axis). The imaginary (in-plane) component of the wave vector, K (ξ) lies along Oz (Ox). The calculated path, with the symbols referring to the points on the loop, connects two symmetrical spots where the D'yakonov-Perel' sub-bands collapse (DP symbols), located in the north (shaded area) and south hemispheres. The departure location in the north hemisphere lies at the colatitude Θ_{DP}.

Now, let us consider the state $|\psi\rangle=|f\rangle\uparrow+|g\rangle\downarrow$ where $|f\rangle$ and $|g\rangle$ are two kets in r-space, i.e., $\langle\mathbf{r}|f\rangle=f(\mathbf{r})$, $\langle\mathbf{r}|g\rangle=g(\mathbf{r})$, and $\psi(r,\sigma)=\langle\mathbf{r}|\psi\rangle=f(\mathbf{r})\uparrow+g(\mathbf{r})\downarrow$. The normalization of the wave vector implies $\langle\psi|\psi\rangle=\langle f|f\rangle+\langle g|g\rangle=1$. We have $\langle\hat{\sigma}_j\rangle=\int\psi^*(r,\sigma)\hat{\sigma}_j\psi(r,\sigma)\mathrm{d}^3\mathbf{r}$, so that

$$\langle\psi|\hat{\boldsymbol{\sigma}}|\psi\rangle^2=1+4[|\langle f|g\rangle|^2-\|f\|^2\|g\|^2]\geq 0. \quad (1)$$

The Cauchy-Schwartz inequality states that $|\langle f|g\rangle|-\|f\|\|g\|\leq 0$ so that the modulus of the spin vector in a mixed state is, in general, smaller than 1. Its norm remains equal to unity if and only if the (f,g) family is not free, i.e., in a pure spin state.

In many usual cases—for instance when f and g relate to different bands of the Hamiltonian without spin—f and g are orthogonal, then

$$\langle\psi|\hat{\boldsymbol{\sigma}}|\psi\rangle^2=1-4\|f\|^2\|g\|^2=4\left(\|f\|^2-\frac{1}{2}\right)^2. \quad (2)$$

If $\|f\|=\|g\|$, we have $\langle\psi|\hat{\boldsymbol{\sigma}}|\psi\rangle^2=0$. This means that, if a band associated with a given spin becomes fully hybridized with another band of opposite spin, with an equal weight for each of the two spin bands, the mean spin modulus becomes zero.

Assume that $|f\rangle$ and $|g\rangle$ belong to a vectorial subspace $\mathcal{E}_n$ with $\dim\mathcal{E}_n=n$, sustended by the orthonormal basis $\mathcal{B}_n$. More formally, the Pauli operator $\hat{\mathfrak{S}}=\hat{\boldsymbol{\sigma}}\otimes\widehat{I_n}$, where $\widehat{I_n}$ is the identity operator acting over $\mathcal{E}_n$, is to be used to calculate the spin vector with $\langle\psi|\hat{\boldsymbol{\sigma}}|\psi\rangle=\langle\psi|\hat{\mathfrak{S}}|\psi\rangle$. The calculation could be performed in the basis $\{\uparrow,\downarrow\}\otimes\mathcal{B}_n$, and in this tensorial-product basis, the matrix representing $\hat{\mathfrak{S}}_j$ is the $(2n\times 2n)$ matrix consisting of n (2×2) identical diagonal blocs, each of them being equal to σ_j. When the spin-orbit coupling is taken into account, $\{\uparrow,\downarrow\}\otimes\mathcal{B}_n$ is not a convenient basis and, depending on the Hamiltonian, another basis involving hybridized states will be used instead. Then, the matrices $\mathfrak{S}_j$ representing $\hat{\mathfrak{S}}$ in this basis will take a more complicated form but, obviously verify the same commutation relations as well as $\mathrm{Tr}\,\mathfrak{S}_j=n\,\mathrm{Tr}\,\sigma_j=0$ and $\det\mathfrak{S}_j=(\det\sigma_j)^n=(-1)^n$.

To study the spin motion along an evanescent band, we calculate the mean value of the Pauli operator in the eigenvector $|\psi\rangle$ corresponding to the energy E. The energy is calculated from the (14×14) Hamiltonian and the eigenvector can be written $|\psi\rangle=\Sigma_{\ell=1}^{14}c_\ell|\Phi_\ell\rangle$ where $\{|\Phi_\ell\rangle\}$ is the set of normalized vectors allowing us to express the (14×14) Hamiltonian. The $|\Phi_\ell\rangle$ are spinors which may be expanded on the $\{\uparrow,\downarrow\}$ basis. The orbital part is written in the basis $\{X,Y,Z,S,X_C,Y_C,Z_C\}$ where X, Y, and Z refer to Γ_{5V}, S refers to Γ_1 symmetry, and X_C, Y_C, and Z_C refer to Γ_{5C}. The detail of the $\mathbf{k}\cdot\mathbf{p}$ matrices up to (30×30) is given in Ref. 10. For convenience, the (14×14) Hamiltonian—similar to the expression derived by Pfeffer and Zawadzki[11] but not identical because the basis differs—is reproduced in the Appendix. We have

$$\langle\psi|\hat{\mathfrak{S}}|\psi\rangle=\sum_{\ell,n=1}^{14}c_\ell^*c_n\langle\Phi_\ell|\hat{\mathfrak{S}}|\Phi_n\rangle=\sum_j\mathbf{e}_j\sum_{\ell,n=1}^{14}c_\ell^*\mathfrak{S}_j^{\ell,n}c_n, \quad (3)$$

where $\mathbf{e}_j$ is the unit vector in the j direction. From the wave functions, the $\mathfrak{S}_j^{\ell,n}$ matrix elements can be straightforwardly calculated. We express them using the (14×14) $[\mathfrak{S}_j]^{\ell,n}$ matrices

$$\mathfrak{S}_j=\begin{pmatrix}\sigma_j^A & 0 & 0\\ 0 & \sigma_j^C & 0\\ 0 & 0 & \sigma_j^B\end{pmatrix}. \quad (4)$$

Here, $\sigma_j^C=\sigma_j$ acts in the conduction (C) $\Gamma_1\otimes\{\uparrow,\downarrow\}=\{|S\rangle\uparrow,|S\rangle\downarrow\}$ subset; σ_j^A acts in the antibonding (A) $\Gamma_{5C}\otimes\{\uparrow,\downarrow\}$ subset, whereas $\sigma_j^B=\sigma_j^A$ acts in the bonding (B) $\Gamma_{5V}\otimes\{\uparrow,\downarrow\}$ subset. For $j=x$ or y, we find

$$\sigma_j^{A,B} = \begin{pmatrix} 0 & e^{-i\varphi_j}/\sqrt{3} & 0 & 0 & -\sqrt{2/3}e^{-i\varphi_j} & 0 \\ e^{i\varphi_j}/\sqrt{3} & 0 & 2e^{-i\varphi_j}/3 & 0 & 0 & -\sqrt{2}e^{-i\varphi_j}/3 \\ 0 & 2e^{i\varphi_j}/3 & 0 & e^{-i\varphi_j}/\sqrt{3} & \sqrt{2}e^{i\varphi_j}/3 & 0 \\ 0 & 0 & e^{i\varphi_j}/\sqrt{3} & 0 & 0 & \sqrt{2/3}e^{i\varphi_j} \\ -\sqrt{2/3}e^{i\varphi_j} & 0 & \sqrt{2}e^{-i\varphi_j}/3 & 0 & 0 & -e^{-i\varphi_j}/3 \\ 0 & -\sqrt{2}e^{i\varphi_j}/3 & 0 & \sqrt{2/3}e^{-i\varphi_j} & -e^{i\varphi_j}/3 & 0 \end{pmatrix} \tag{5}$$

with $\varphi_x=0$ and $\varphi_y=\pi/2$. For $j=z$, we obtain

$$\sigma_z^{A,B} = \begin{pmatrix} 1 & 0 & 0 & 0 & 0 & 0 \\ 0 & 1/3 & 0 & 0 & 2\sqrt{2}/3 & 0 \\ 0 & 0 & -1/3 & 0 & 0 & 2\sqrt{2}/3 \\ 0 & 0 & 0 & -1 & 0 & 0 \\ 0 & 2\sqrt{2}/3 & 0 & 0 & -1/3 & 0 \\ 0 & 0 & 2\sqrt{2}/3 & 0 & 0 & 1/3 \end{pmatrix}. \tag{6}$$

The results need a numerical calculation because $\{c_n\}$ is to be determined. However, for complex wave vectors with a small modulus, analytical solutions can be derived and it is illuminating to consider this case. Near the Brillouin-zone center, the energy dispersion of the first conduction band is accurately described by the DP Hamiltonian, $\hat{H}_{DP}$, which can be obtained from the (14×14) Hamiltonian performing a third-order perturbation expansion from remote bands

$$\hat{H}_{DP} = \gamma_c \mathbf{k}^2 + \gamma \boldsymbol{\chi} \cdot \hat{\boldsymbol{\sigma}}, \tag{7}$$

where γ is the coupling parameter and $\gamma_c=\hbar^2/2m$, with m being the effective mass; $\boldsymbol{\chi}=\boldsymbol{\chi}(\mathbf{k})$ is a vector representing the internal field, $[\chi_x,\chi_y,\chi_z]=[k_x(k_y^2-k_z^2),k_y(k_z^2-k_x^2),k_z(k_x^2-k_y^2)]$. The H_{DP} matrix is expressed in the $\{|S\rangle\uparrow,|S\rangle\downarrow\}$ basis. The evanescent states that we are studying correspond to wave vectors of the form $\{\alpha(\boldsymbol{\xi}+i\beta\mathbf{K})=\alpha(\xi\mathbf{e}_x+i\beta K\mathbf{e}_z);\alpha,\beta=\pm 1\}$. Note that α and β only take the values +1 or −1: $\alpha=1$, $\beta=1(-1)$ refer to the wave-vector $\mathbf{k}$ ($\mathbf{k}^*$) whereas $\alpha=-1$, $\beta=1(-1)$ refer to the wave vector $-\mathbf{k}$ ($-\mathbf{k}^*$). We use the notation $\eta=\xi/K=\tan\theta$ so that $\mathbf{k}=K[\alpha\eta,0,i\alpha\beta]$. Now, the DP field is $\boldsymbol{\chi}=K^3[\alpha\eta,0,i\alpha\beta\eta^2]$ and H_{DP} can be written as

$$H_{DP} = \begin{bmatrix} \gamma_c k^2 + i\alpha\beta\gamma\eta^2K^3 & \alpha\gamma\eta K^3 \\ \alpha\gamma\eta K^3 & \gamma_c k^2 - i\alpha\beta\gamma\eta^2K^3 \end{bmatrix}. \tag{8}$$

For a given wave-vector $\mathbf{k}$, H_{DP} has the two eigenvalues $\lambda_\pm=\gamma_c k^2+\epsilon\gamma\eta\sqrt{1-\eta^2}K^3$, $\epsilon=\pm 1$ correspond to the two energies of two spin states, we shall see the meaning of which just below. Observe that on a real-energy line we have $\eta<1$ (i.e., $\theta<45°$). The components of the corresponding eigenstates are $a=1/\sqrt{2}$ and $b=(\epsilon\alpha\sqrt{1-\eta^2}-i\beta\eta)/\sqrt{2}$. We calculate $\langle\hat{\sigma}_x\rangle=\epsilon\alpha\sqrt{1-\eta^2}$, $\langle\hat{\sigma}_y\rangle=-\beta\eta$, and $\langle\hat{\sigma}_z\rangle=0$. This shows that the spin remains in the xOy plane, perpendicular to the z-quantization axis. In GaAs, γ is a negative quantity[12] so that $\epsilon=-1$ ($\epsilon=+1$) corresponds to the higher- (lower-) energy sub-band. Let us define $\mathbf{n}_\pm=[\sqrt{1-\eta^2},\pm\eta,0]$. The unit vector $\mathbf{n}_+$ makes the angle Θ_{DP} with respect to Ox, with $\sin\Theta_{DP}=\eta=\tan\theta$. The result is summed up in Table I, which indicates $\langle\hat{\boldsymbol{\sigma}}\rangle$ for a given wave vector at a given ϵ.

These two spins are not collinear unless $\eta=0$ (and, in this latter case, the spin splitting of the evanescent states vanishes). Note that in the DP case the quantum state is $|\varphi\rangle=a|S\rangle\uparrow+b|S\rangle\downarrow$ and then the norm of the spin vector is equal to 1.

When going off the Brillouin-zone center, H_{DP} can no longer be used so that a numerical calculation has to be performed as explained above. The GaAs $\mathbf{k}\cdot\mathbf{p}$ parameter values used in the present calculation are $P=9.88$ eV.Å, $P'=0.41$ eV.Å, $E_G=1.519$ eV, $\Delta_C=E_{\Gamma_{8C}}-E_{\Gamma_{7C}}=0.171$ eV, $Q=8.68$ eV.Å, $\Delta=0.341$ eV, $E_\Delta=E_{\Gamma_{7C}}-E_{\Gamma_6}=2.969$ eV, and $\Delta'=-0.17$ eV.[13] This parameter set yields $\gamma=-24$ eV.Å^3. To obtain an image of the spin evolution, it is convenient to plot the spin vector along the loop as shown in Fig. 1. In the upper part, the evanescent loop describes the energy for $\eta=\xi/K=0.4$ ($\theta=21.8°$). All the spin vectors drawn on the curve result from numerical calculation, the DP limit being out of the representation domain. In the lower part, the spin path is drawn on the sphere, the spin modulus being almost constant within an accuracy of 3%. As underlined in Sec. II, it is not obvious that the spin motion can be represented on the unit sphere because, in an hybridized band, the spin vector has a modulus smaller than 1, and possibly 0. The quasiconservation of the modulus is essential for applications to spintronics. Near the Brillouin-zone center, the spin-vector $\mathbf{n}_-$ in the lower-energy sub-band ($\epsilon=+1$) starts from a direction at the polar angle Θ_{DP} with respect to Ox. More precisely, on the unit sphere with the north pole defined by Ox and the longitude of 0° corresponding to the Oy axis, $\mathbf{n}_-$ is defined by the colatitude Θ_{DP} and a longitude of 180°. When increasing the wave-vector modulus, the spin vector rotates at a constant longitude to make the angle Θ with respect to Ox. Starting from the $\Theta=\Theta_{DP}$ in the DP regime, Θ increases up to a point where the spin vector lies along Oy ($\Theta=90°$). Having in mind a movement on the sphere, the path first occurs in the north hemisphere (shaded area). It starts from a point at the colatitude Θ_{DP} which increases versus θ ($\Theta_{DP}\approx\theta$ within an accuracy of 10% up to about 25°, and $\Theta_{DP}=90°$ for $\theta=45°$, the maximum possible value) to reach the equatorial plane $\Theta=90°$. When θ is small but nonzero, the departure point lies near the north pole, but never exactly at the pole. Crossing the

TABLE I. Spin vector $\langle\hat{\boldsymbol{\sigma}}\rangle$ in the D'yakonov-Perel' sub-bands ($\epsilon=\pm1$) and relevant wave vectors. $\mathbf{n}_{\pm}$ are unit vectors that are not collinear.

	$\epsilon=+1$	$\epsilon=-1$
$\mathbf{k}$	$\mathbf{n}_{-}$	$-\mathbf{n}_{+}$
$-\mathbf{k}$	$-\mathbf{n}_{+}$	$\mathbf{n}_{-}$
$\mathbf{k}^{*}$	$\mathbf{n}_{+}$	$-\mathbf{n}_{-}$
$-\mathbf{k}^{*}$	$-\mathbf{n}_{-}$	$\mathbf{n}_{+}$

equatorial plane, the x component of the spin vector becomes negative and the path lies in the south hemisphere: the spin continues to rotate to reach a point which is symmetrical to the departure position with respect to the equatorial plane. This last location is reached in the small-wave-vector regime for $\epsilon=-1$ and the spin vector is $-\mathbf{n}_{+}$. Alternatively, one may think of two spin sub-bands near the zone center which extend off the zone center to connect at the equator. At large θ, not far from 45°, the departure and arrival locations come close to the equator: the length of the path becomes shorter and shorter, tending to zero and it can be seen that, correlatively, the length of the evanescent loop decreases to zero.[4] In Ref. 7, tunneling of electrons under off-normal incidence on a [001]-oriented barrier (z axis) was analyzed, taking ξ along Ox. Then, the tunnel scheme involves two evanescent loops in the xOz plane, because, at a given energy the ξ component of the wave vector has to be conserved, leading to two different θ angles corresponding to wave-vector components K and K' in each "spin" sub-band. As a result, and in agreement with the calculation by Perel' *et al.*,[9] the barrier acts as a spin filter. Fig. 1 in the present paper is also drawn with reference to this very situation: the Oz axis is the tunneling direction—the loop lies in the xOz plane, and Ox is the "spin-filter axis." Roughly speaking, the transmission asymmetry, which is also the transmitted beam polarization when the primary beam is unpolarized, is equal to $\tanh[(aK)(\delta K/K)]$.[7] In this expression (aK) determines the barrier transmission and $(\delta K/K)$ is the "initial" polarization of the sub-bands. We have the relation $d\theta=-\cos^2\theta(\xi/K)(dK/K)$, which shows that, when the ratio ξ/K is small, $d\theta$ is a second-order term which can be neglected. Therefore, δK simply corresponds to the distance between the two branches of the loop at a given energy, restoring a familiar picture. In Fig. 1, it can be shown that, along the loop, $\delta K/K$ starts from the value $(\gamma/\gamma_c)K\tan\theta$ to reach about 7% at $\|\mathbf{k}\|=K/\cos\theta\approx0.1(2\pi/a_0)$ while the spin vector only slightly changes. Therefore, it can be expected that transmission asymmetries as large as 20 % could be achieved, instead of 2 % in the DP limit for a 40 Å-thick barrier. In GaSb, the ratio (γ/γ_c) is about five times larger than in GaAs (Ref. 13) so that extremely high polarizations might be expected.

III. CONCLUSION

In conclusion, the loop structure of the spin sub-bands along $[\tan\theta,0,i]$ directions is responsible for the spin-filtering capability of a [001]-oriented GaAs barrier under off-normal incidence. The θ angle defines the in-plane component ξ of the wave vector—a quantity which is conserved in the tunnel process—through the relation $\tan\theta=\xi/K$, where K is the imaginary component of the wave vector in the barrier. This peculiar topology is a consequence of the spin-orbit interaction in the absence of inversion symmetry. A complete analysis of the spin-vector trajectory has been performed and, if the result is simple, it is far from intuitive. For a wave-vector K $[\tan\theta,0,i]$ at a fixed θ value, the two sub-bands which originate from the diagonalization of the D'yakonov-Perel' Hamiltonian, that we call the DP sub-bands, do not correspond to opposite spin states, even infinitely close to the Brillouin-zone center. Representing the spin vector on the unit sphere, these DP sub-bands reduce to two points located at the same longitude, which are symmetrical with respect to the equatorial plane. Their colatitude Θ_{DP} which varies between 0 and 90°, depends on θ, which varies between 0 and 45°: at small angles $\Theta_{DP}\approx\theta$ whereas Θ_{DP} rapidly increases at large θ. The loops in the dispersion relation of the evanescent bands correspond to paths which connect these two DP spots at the equator when K is large enough. The spin tag allows us to define properly the point where the two sub-bands, which might be thought as up- and down-spin sub-bands near the zone center, connect because one path entirely lies into the north hemisphere (along this path, the spin is rather up than down) whereas the other entirely lies into the south hemisphere (in this region, the spin is rather down than up). In the tunneling geometry, at a fixed energy, the wave with wave-vector $\mathbf{k}$ has to be associated to the wave with wave-vector $\mathbf{k}^{*}$ and it is obvious that these two waves do not correspond to identical spin states so that a two spin-channel tunneling model has to be used to account for electron transmission.[7] Besides, when going off the zone center, the bands hybridize, the spin is no longer a good quantum number and the modulus of the spin vector is slightly reduced. These peculiarities correspond to a situation that appears to be quite general in solids.

ACKNOWLEDGMENT

We thank Travis Wade for a critical reading of the manuscript.

APPENDIX: THE (14×14) HAMILTONIAN

Let X, Y, and Z be the orbital functions of the Γ_{5V} valence band (at $\mathbf{k}=\mathbf{0}$, without spin-orbit interaction) in Koster's notations.[14] Due to spin-orbit interaction the Γ_{5V} level splits into Γ_{8V} and Γ_{7V} subsets. To save place, the four Γ_{8V} functions are referred to as $|M\rangle$ with $M=\pm\frac{3}{2},\pm\frac{1}{2}$ while the two Γ_{7V} functions are written as $|\pm\frac{7}{2}\rangle$, a mnemonic notation recalling that these last two functions belong to Γ_{7V}. S is the orbital function of the first conduction-band Γ_1. X_C, Y_C, and Z_C are the orbital functions of the second conduction-band Γ_{5C}. Due to spin-orbit interaction the Γ_{5C} level splits into Γ_{8C} and Γ_{7C} subsets. The four Γ_{8C} functions are written as

$|cM\rangle$ and the two Γ_{7C} functions are written as $|c\frac{\pm 7}{2}\rangle$.

When one has to deal with time-reversal operator $\hat{\mathbf{K}} = -i\sigma_y \hat{K}_0$, where σ_y is the relevant Pauli matrix and $\hat{K}_0$ is the operation of taking the complex conjugate—as done in Ref. 7—it is preferable to use the basis defined in Ref. 15. Thus, we construct the basis given in Table II where the atomic functions φ_s, φ_{p_x}, φ_{p_y}, and φ_{p_z} of Ref. 15 are substituted with S, X, Y, and Z. Then, the (14×14) Hamiltonian writes:

$$
\begin{array}{c}
\begin{array}{cccccccccccccc}
\left|c\frac{3}{2}\right\rangle & \left|c\frac{1}{2}\right\rangle & \left|c\frac{-1}{2}\right\rangle & \left|c\frac{-3}{2}\right\rangle & \left|c\frac{7}{2}\right\rangle & \left|c\frac{-7}{2}\right\rangle & |+\rangle & |-\rangle & \left|\frac{3}{2}\right\rangle & \left|\frac{1}{2}\right\rangle & \left|\frac{-1}{2}\right\rangle & \left|\frac{-3}{2}\right\rangle & \left|\frac{7}{2}\right\rangle & \left|\frac{-7}{2}\right\rangle
\end{array} \\
\left[\begin{array}{cccccccccccccc}
E_{8C}^H & \mathfrak{B}_C & \mathfrak{C}_C & 0 & \frac{1}{\sqrt{2}}\mathfrak{B}_C & \sqrt{2}\mathfrak{C}_C & \frac{-1}{\sqrt{2}}P'^- & 0 & \frac{1}{3}\Delta' & \frac{1}{\sqrt{3}}P_X^+ & \frac{1}{\sqrt{3}}P_X^z & 0 & \frac{1}{\sqrt{6}}P_X^+ & \sqrt{\frac{2}{3}}P_X^z \\
\mathfrak{B}_C^* & E_{8C}^L & 0 & \mathfrak{C}_C & -\sqrt{2}\mathfrak{A}_C & -\sqrt{\frac{3}{2}}\mathfrak{B}_C & \sqrt{\frac{2}{3}}P'^z & \frac{-1}{\sqrt{6}}P'^- & \frac{-1}{\sqrt{3}}P_X^- & \frac{1}{3}\Delta' & 0 & \frac{1}{\sqrt{3}}P_X^z & 0 & \frac{-1}{\sqrt{2}}P_X^+ \\
\mathfrak{C}_C^* & 0 & E_{8C}^L & -\mathfrak{B}_C & -\sqrt{\frac{3}{2}}\mathfrak{B}_C^* & \sqrt{2}\mathfrak{A}_C & \frac{1}{\sqrt{6}}P'^+ & \sqrt{\frac{2}{3}}P'^z & \frac{-1}{\sqrt{3}}P_X^z & 0 & \frac{1}{3}\Delta' & \frac{-1}{\sqrt{3}}P_X^+ & \frac{1}{\sqrt{2}}P_X^- & 0 \\
0 & \mathfrak{C}_C^* & -\mathfrak{B}_C^* & E_{8C}^H & -\sqrt{2}\mathfrak{C}_C^* & \frac{1}{\sqrt{2}}\mathfrak{B}_C^* & 0 & \frac{1}{\sqrt{2}}P'^+ & 0 & \frac{-1}{\sqrt{3}}P_X^z & \frac{1}{\sqrt{3}}P_X^- & \frac{1}{3}\Delta' & \sqrt{\frac{2}{3}}P_X^z & \frac{-1}{\sqrt{6}}P_X^- \\
\frac{1}{\sqrt{2}}\mathfrak{B}_C^* & -\sqrt{2}\mathfrak{A}_C & -\sqrt{\frac{3}{2}}\mathfrak{B}_C & -\sqrt{2}\mathfrak{C}_C & E_{7C}^k & 0 & \frac{1}{\sqrt{3}}P'^z & \frac{1}{\sqrt{3}}P'^- & \frac{-1}{\sqrt{6}}P_X^- & 0 & \frac{-1}{\sqrt{2}}P_X^+ & -\sqrt{\frac{2}{3}}P_X^z & \frac{-2}{3}\Delta' & 0 \\
\sqrt{2}\mathfrak{C}_C^* & -\sqrt{\frac{3}{2}}\mathfrak{B}_C^* & \sqrt{2}\mathfrak{A}_C & \frac{1}{\sqrt{2}}\mathfrak{B}_C & 0 & E_{7C}^k & \frac{1}{\sqrt{3}}P'^+ & \frac{-1}{\sqrt{3}}P'^z & -\sqrt{\frac{2}{3}}P_X^z & \frac{1}{\sqrt{2}}P_X^- & 0 & \frac{1}{\sqrt{6}}P_X^+ & 0 & \frac{-2}{3}\Delta' \\
\frac{-1}{\sqrt{2}}P'^+ & \sqrt{\frac{2}{3}}P'^z & \frac{1}{\sqrt{6}}P'^- & 0 & \frac{1}{\sqrt{3}}P'^z & \frac{1}{\sqrt{3}}P'^- & E_6^k & 0 & \frac{-1}{\sqrt{2}}P^+ & \sqrt{\frac{2}{3}}P^z & \frac{1}{\sqrt{6}}P^- & 0 & \frac{1}{\sqrt{3}}P^z & \frac{1}{\sqrt{3}}P^- \\
0 & \frac{-1}{\sqrt{6}}P'^+ & \sqrt{\frac{2}{3}}P'^z & \frac{1}{\sqrt{2}}P'^- & \frac{1}{\sqrt{3}}P'^+ & \frac{-1}{\sqrt{3}}P'^z & 0 & E_6^k & 0 & \frac{-1}{\sqrt{6}}P^+ & \sqrt{\frac{2}{3}}P^z & \frac{1}{\sqrt{2}}P^- & \frac{1}{\sqrt{3}}P^+ & \frac{-1}{\sqrt{3}}P^z \\
\frac{1}{3}\Delta' & \frac{-1}{\sqrt{3}}P_X^+ & \frac{-1}{\sqrt{3}}P_X^z & 0 & \frac{-1}{\sqrt{6}}P_X^+ & -\sqrt{\frac{2}{3}}P_X^z & \frac{-1}{\sqrt{2}}P^- & 0 & E_8^H & \mathfrak{B} & \mathfrak{C} & 0 & \frac{1}{\sqrt{2}}\mathfrak{B} & \sqrt{2}\mathfrak{C} \\
\frac{1}{\sqrt{3}}P_X^- & \frac{1}{3}\Delta' & 0 & \frac{-1}{\sqrt{3}}P_X^z & 0 & \frac{1}{\sqrt{2}}P_X^+ & \sqrt{\frac{2}{3}}P^z & \frac{-1}{\sqrt{6}}P^- & \mathfrak{B}^* & E_8^L & 0 & \mathfrak{C} & -\sqrt{2}\mathfrak{A} & -\sqrt{\frac{3}{2}}\mathfrak{B} \\
\frac{1}{\sqrt{3}}P_X^z & 0 & \frac{1}{3}\Delta' & \frac{1}{\sqrt{3}}P_X^+ & \frac{-1}{\sqrt{2}}P_X^- & 0 & \frac{1}{\sqrt{6}}P^+ & \sqrt{\frac{2}{3}}P^z & \mathfrak{C}^* & 0 & E_8^L & -\mathfrak{B} & -\sqrt{\frac{3}{2}}\mathfrak{B}^* & \sqrt{2}\mathfrak{A} \\
0 & \frac{1}{\sqrt{3}}P_X^z & \frac{-1}{\sqrt{3}}P_X^- & \frac{1}{3}\Delta' & -\sqrt{\frac{2}{3}}P_X^z & \frac{1}{\sqrt{6}}P_X^- & 0 & \frac{1}{\sqrt{2}}P^+ & 0 & \mathfrak{C}^* & -\mathfrak{B}^* & E_8^H & -\sqrt{2}\mathfrak{C}^* & \frac{1}{\sqrt{2}}\mathfrak{B}^* \\
\frac{1}{\sqrt{6}}P_X^- & 0 & \frac{1}{\sqrt{2}}P_X^+ & \sqrt{\frac{2}{3}}P_X^z & \frac{-2}{3}\Delta' & 0 & \frac{1}{\sqrt{3}}P^z & \frac{1}{\sqrt{3}}P^- & \frac{1}{\sqrt{2}}\mathfrak{B}^* & -\sqrt{2}\mathfrak{A} & -\sqrt{\frac{3}{2}}\mathfrak{B} & -\sqrt{2}\mathfrak{C} & E_7^k & 0 \\
\sqrt{\frac{2}{3}}P_X^z & \frac{-1}{\sqrt{2}}P_X^- & 0 & \frac{-1}{\sqrt{6}}P_X^+ & 0 & \frac{-2}{3}\Delta' & \frac{1}{\sqrt{3}}P^+ & \frac{-1}{\sqrt{3}}P^z & \sqrt{2}\mathfrak{C}^* & -\sqrt{\frac{3}{2}}\mathfrak{B}^* & \sqrt{2}\mathfrak{A} & \frac{1}{\sqrt{2}}\mathfrak{B} & 0 & E_7^k
\end{array}\right]
\end{array}
\tag{A1}
$$

In Eq. (A1), the parameters are the following:

$$P = (\hbar/m_0)\langle S|p_x|iX\rangle;$$

$$P_X = (\hbar/m_0)\langle X_C|p_y|iZ\rangle;$$

$$P' = (\hbar/m_0)\langle S|p_x|iX_C\rangle.$$

m_0 is the free-electron mass. P, P_X, and P' are real.

$$P_\alpha^\pm = P_\alpha(k_x \pm ik_y), \quad P_\alpha^z = P_\alpha k_z$$

with $P_\alpha = P$ or P_X or P'.

$$E_{P\alpha} = (2m_0/\hbar^2)P_\alpha^2.$$

$$\Delta = (3\hbar/4m_0^2c^2)\langle X|(\partial\mathfrak{U}/\partial x)p_y - (\partial\mathfrak{U}/\partial y)p_x|iY\rangle;$$

$$\Delta_C = (3\hbar/4m_0^2c^2)\langle X_C|(\partial\mathfrak{U}/\partial x)p_y - (\partial\mathfrak{U}/\partial y)p_x|iY_C\rangle;$$

$$\Delta' = (3\hbar/4m_0^2c^2)\langle X|(\partial\mathfrak{U}/\partial x)p_y - (\partial\mathfrak{U}/\partial y)p_x|iY_C\rangle.$$

$\mathfrak{U}$ is the periodic potential in the Bloch Hamiltonian $\mathbf{p}^2/2m_0 + \mathfrak{U}(\mathbf{r})$. Δ, Δ_C, and Δ' are, respectively, the spin-orbit-coupling energy of the Γ_{5V} valence band which results in Γ_{8V} and Γ_{7V}, the spin-orbit-coupling energy of the second Γ_{5C} conduction band which results in Γ_{8C} and Γ_{7C}, and the interband spin-orbit-coupling energy between Γ_{5V} and Γ_{5C}.

P' and Δ' vanish in O_h group but are nonzero in T_d group.

$$E_{8C}^H = E'_{8C} - \gamma'_{C1}\check{k}^2 + \mathfrak{A}_C; \quad E_{8C}^L = E'_{8C} - \gamma'_{C1}\check{k}^2 - \mathfrak{A}_C;$$
$$E_{7C}^k = E'_{7C} - \gamma'_{C1}\check{k}^2; \quad E'_{8C} - E'_{7C} = \Delta_C;$$

$$E_6^k = E_6 + \gamma'_C\check{k}^2;$$

$$E_8^H = E'_8 - \gamma'_1\check{k}^2 + \mathfrak{A}; \quad E_8^L = E'_8 - \gamma'_1\check{k}^2 - \mathfrak{A};$$
$$E_7^k = E'_7 - \gamma'_1\check{k}^2; \quad E'_8 - E'_7 = \Delta.$$

$$\mathfrak{A}_C = \gamma'_{C2}(2\check{k}_z^2 - \check{k}_\rho^2); \quad \mathfrak{B}_C = 2\sqrt{3}\gamma'_{C3}\check{k}_z\check{k}_-;$$
$$\mathfrak{C}_C = \sqrt{3}[\gamma'_{C2}(\check{k}_x^2 - \check{k}_y^2) - 2i\gamma'_{C3}\check{k}_x\check{k}_y];$$

TABLE II. The basis wave functions of the (14×14) Hamiltonian. These functions are pairs of Kramers conjugates. For example, $\hat{\mathbf{K}}|+\rangle=|-\rangle$ or $\hat{\mathbf{K}}|\frac{3}{2}\rangle=|\frac{-3}{2}\rangle$.

$\|+\rangle=\|S\uparrow\rangle$	$\|-\rangle=\|S\downarrow\rangle$
$\|c\frac{3}{2}\rangle=\|i[-\sqrt{1/2}(X_C+iY_C)\uparrow]\rangle$	$\|\frac{3}{2}\rangle=\|i[-\sqrt{1/2}(X+iY)\uparrow]\rangle$
$\|c\frac{1}{2}\rangle=\|i[\sqrt{2/3}Z_C\uparrow-\sqrt{1/6}(X_C+iY_C)\downarrow]\rangle$	$\|\frac{1}{2}\rangle=\|i[\sqrt{2/3}Z\uparrow-\sqrt{1/6}(X+iY)\downarrow]\rangle$
$\|c\frac{-1}{2}\rangle=\|i[\sqrt{1/6}(X_C-iY_C)\uparrow+\sqrt{2/3}Z_C\downarrow]\rangle$	$\|\frac{-1}{2}\rangle=\|i[\sqrt{1/6}(X-iY)\uparrow+\sqrt{2/3}Z\downarrow]\rangle$
$\|c\frac{-3}{2}\rangle=\|i[\sqrt{1/2}(X_C-iY_C)\downarrow]\rangle$	$\|\frac{-3}{2}\rangle=\|i[\sqrt{1/2}(X-iY)\downarrow]\rangle$
$\|c\frac{7}{2}\rangle=\|i[\sqrt{1/3}Z_C\uparrow+\sqrt{1/3}(X_C+iY_C)\downarrow]\rangle$	$\|\frac{7}{2}\rangle=\|i[\sqrt{1/3}Z\uparrow+\sqrt{1/3}(X+iY)\downarrow]\rangle$
$\|c\frac{-7}{2}\rangle=\|i[\sqrt{1/3}(X_C-iY_C)\uparrow-\sqrt{1/3}Z_C\downarrow]\rangle$	$\|\frac{-7}{2}\rangle=\|i[\sqrt{1/3}(X-iY)\uparrow-\sqrt{1/3}Z\downarrow]\rangle$

$$\mathfrak{A}=\gamma_2'(2\check{k}_z^2-\check{k}_\rho^2);\quad \mathfrak{B}=2\sqrt{3}\gamma_3'\check{k}_z\check{k}_-;$$

$$\mathfrak{C}=\sqrt{3}[\gamma_2'(\check{k}_x^2-\check{k}_y^2)-2i\gamma_3'\check{k}_x\check{k}_y].$$

$$\check{k}_w=\sqrt{\hbar^2/2m_0}k_w \quad \text{with} \quad w=x,y,z.$$

$$\check{k}_\pm=\check{k}_x\pm i\check{k}_y,\ \check{k}_\rho^2=\check{k}_x^2+\check{k}_y^2.$$

E_{8C}', E_{7C}', E_8', and E_7' would, respectively, be the energies $E(\Gamma_{8C})$, $E(\Gamma_{7C})$, $E(\Gamma_{8V})$, and $E(\Gamma_{7V})$ at $\mathbf{k}=\mathbf{0}$ if the Δ' interband spin-orbit coupling were equal to zero.

Furthermore,

$$\gamma_C'=\gamma_C-\frac{E_P}{3}\left(\frac{2}{E_G}+\frac{1}{E_G+\Delta}\right)+\frac{E_P'}{3}\left(\frac{2}{E_{8C-6}}+\frac{1}{E_{7C-6}}\right),$$

$$\gamma_1'=\gamma_1-\frac{E_P}{3E_G}-\frac{E_{PX}}{3}\left(\frac{1}{E_{7C-8}}+\frac{1}{E_{8C-8}}\right),$$

$$\gamma_2'=\gamma_2-\frac{E_P}{6E_G}+\frac{E_{PX}}{6E_{7C-8}},$$

$$\gamma_3'=\gamma_3-\frac{E_P}{6E_G}-\frac{E_{PX}}{6E_{7C-8}}, \tag{A2}$$

where E_G is the band-gap energy and $E_{n-m}=E(\Gamma_n)-E(\Gamma_m)$.

As quoted in Ref. 11, γ_j' $(j=1,2,3)$ are Luttinger-like parameters, in which the $\mathbf{k}\cdot\mathbf{p}$ interaction inside $\{\Gamma_{8C},\Gamma_{7C},\Gamma_6,\Gamma_{8V},\Gamma_{7V}\}$ has been subtracted. γ_j are Luttinger parameters. The same holds for γ_{Cj}'. However and for the sake of simplicity we take γ_{Cj}' equal to zero which does not change any significant result for the spin splitting in the forbidden band gap as shown in Ref. 4. In the same way, γ_C' is linked to γ_c with $\gamma_C=m_0/m_C$ where m_C is the conduction effective mass.

*henri-jean.drouhin@polytechnique.edu

[1] W. H. Butler, X.-G. Zhang, T. C. Schulthess, and J. M. MacLaren, Phys. Rev. B **63**, 054416 (2001); Phys. Rev. B **63**, 092402 (2001).

[2] V. Heine, Proc. Phys. Soc. London **81**, 300 (1963).

[3] R. O. Jones, Proc. Phys. Soc. London **89**, 443 (1966).

[4] S. Richard, H.-J. Drouhin, N. Rougemaille, and G. Fishman, J. Appl. Phys. **97**, 083706 (2005).

[5] N. Rougemaille, H.-J. Drouhin, S. Richard, G. Fishman, and A. K. Schmid, Phys. Rev. Lett. **95**, 186406 (2005).

[6] G. Dresselhaus, Phys. Rev. **100**, 580 (1955).

[7] T. L. Hoai Nguyen, H.-J. Drouhin, J.-E. Wegrowe, and G. Fishman, Phys. Rev. B **79**, 165204 (2009).

[8] M. D'yakonov and V. I. Perel', Zh. Eksp. Teor. Fiz. **60**, 1954 (1971); [Sov. Phys. JETP **33**, 1053 (1971)]; M. D'yakonov and V. I. Perel', Fiz. Tverd. Tela (Leningrad) **13**, 3581 (1971); [Sov. Phys. Solid State **13**, 3023 (1972)].

[9] V. I. Perel', S. A. Tarasenko, I. N. Yassievich, S. D. Ganichev, V. V. Bel'kov, and W. Prettl, Phys. Rev. B **67**, 201304(R) (2003).

[10] G. Fishman, *Semi-conducteurs: les bases de la théorie* $\mathbf{k}\cdot\mathbf{p}$ (Les Éditions de l'École Polytechnique, Palaiseau, 2009).

[11] P. Pfeffer and W. Zawadzki, Phys. Rev. B **53**, 12813 (1996).

[12] B. Jusserand, D. Richards, G. Allan, C. Priester, and B. Etienne, Phys. Rev. B **51**, 4707 (1995).

[13] J.-M. Jancu, R. Scholz, E. A. de Andrada e Silva, and G. C. La Rocca, Phys. Rev. B **72**, 193201 (2005). Δ^- and Δ_0' in the article by Jancu *et al.* are, respectively, written as Δ' and Δ_C in the present article.

[14] G. F. Koster, J. O. Dimmock, G. Wheeler, and R. G. Statz, *Properties of the Thirty-Two Point Groups* (MIT Press, Cambridge, Massachusetts, 1963).

[15] A. Messiah, *Mécanique Quantique* (Dunod, Paris, 1995), p. 445.